










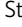

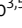
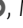




BRIEF DEFINITIVE REPORT

Stunning of neutrophils accounts for the anti-inflammatory effects of clodronate liposomes

Stephan Culemann^{1,2*} , Katharina Knab^{1,2*} , Maximilien Euler^{1,2*} , Anja Wegner^{1,2} , Hilal Garibagaoglu^{1,2} , Jochen Ackermann^{1,2} , Kim Fischer^{1,2} , Deborah Kienhöfer^{1,2} , Georgiana Crainiciuc³ , Jonas Hahn^{1,2} , Anika Grüneboom^{1,2} , Falk Nimmerjahn⁴ , Stefan Uderhardt^{1,2} , Andrés Hidalgo^{3,5} , Georg Schett^{1,2} , Markus H. Hoffmann^{1,2,6*} , and Gerhard Krönke^{1,2*} 

Clodronate liposomes (Clo-Lip) have been widely used to deplete mononuclear phagocytes (MoPh) to study the function of these cells in vivo. Here, we revisited the effects of Clo-Lip together with genetic models of MoPh deficiency, revealing that Clo-Lip exert their anti-inflammatory effects independent of MoPh. Notably, not only MoPh but also polymorphonuclear neutrophils (PMN) ingested Clo-Lip in vivo, which resulted in their functional arrest. Adoptive transfer of PMN, but not of MoPh, reversed the anti-inflammatory effects of Clo-Lip treatment, indicating that stunning of PMN rather than depletion of MoPh accounts for the anti-inflammatory effects of Clo-Lip in vivo. Our data highlight the need for a critical revision of the current literature on the role of MoPh in inflammation.

Introduction

Mononuclear phagocytes (MoPh) including blood monocytes and macrophages comprise heterogeneous populations of cells that fulfill essential roles during homeostasis, inflammation, and host defense (Ginhoux and Jung, 2014). Blood monocytes, which are constantly replenished from bone marrow precursors, can be subdivided into “resident” Ly6C^{low} monocytes and “inflammatory” Ly6C^{high} monocytes (Geissmann et al., 2010). Both subgroups of monocytes show distinct behavior and are considered to fulfill specific and non-redundant functions. Ly6C^{low} monocytes display a patrolling migratory pattern in the vasculature and constantly survey the tissue, whereas Ly6C^{high} monocytes primarily extravasate upon onset of inflammation and represent the major source for subsequently differentiating monocyte-derived macrophages that infiltrate inflamed tissues (Ginhoux and Jung, 2014). Most organs additionally harbor tissue-resident macrophages (TRM) that derive from precursors settling the tissue during the pre- or perinatal period and that self-maintain their numbers largely independent of blood monocytes (Blériot et al., 2020). TRM thus represent the predominant type of macrophages during steady state in organs such as the brain, the liver, or the synovial joints, where they primarily support tissue homeostasis and organ function (Davies et al., 2013).

Despite decades of research, the exact role MoPh exert during tissue homeostasis as well as during the onset and resolution of inflammation remains controversial and Janus-faced. Both monocytes and macrophages were repeatedly suggested to perpetuate tissue damage during chronic inflammatory disorders such as inflammatory bowel disease, multiple sclerosis, or rheumatoid arthritis (RA). At the same time, they have been implicated in the prevention and resolution of inflammation as well as the repair of tissue injury (Bogie et al., 2014; Caër and Wick, 2020; Culemann et al., 2019a; Culemann et al., 2019b; Gordon, 2007; Kurowska-Stolarska and Alivernini, 2017; Solomon et al., 2005; Udalova et al., 2016). Although cellular plasticity and a differential role of individual monocyte and macrophage subsets might account for these seemingly controversial data, there are also considerable methodologic shortcomings in the field of macrophage and monocyte research that currently hinder an unbiased and comprehensive view of the exact role of these cells. Especially, the use of clodronate liposomes (Clo-Lip) as a widely used approach to deplete MoPh in the blood and tissue of mice has generated a considerable amount of data that substantially shaped our understanding of the role of these cells during inflammation (Barrera et al., 2000; Moreno,

¹Department of Internal Medicine 3 - Rheumatology and Immunology, Friedrich-Alexander University Erlangen-Nürnberg and Universitätsklinikum Erlangen, Erlangen, Germany; ²Deutsches Zentrum für Immuntherapie, Friedrich-Alexander University Erlangen-Nürnberg and Universitätsklinikum Erlangen, Erlangen, Germany; ³Area of Cell and Developmental Biology, Centro Nacional de Investigaciones Cardiovasculares Carlos III, Madrid, Spain; ⁴Institute of Genetics at the Department of Biology, Friedrich-Alexander University Erlangen-Nürnberg, Erlangen, Germany; ⁵Vascular Biology and Therapeutics Program and Department of Immunobiology, Yale University School of Medicine, New Haven, CT, USA; ⁶Department of Dermatology, Allergy and Venerology, University of Lübeck, Lübeck, Germany.

*S. Culemann, K. Knab, M. Euler, M.H. Hoffmann, and G. Krönke contributed equally to this paper. Correspondence to Gerhard Krönke: gerhard.kroenke@uk-erlangen.de

Stephan Culemann's current affiliation is Immunology of Aging, Leibniz Institute on Aging – Fritz-Lipmann-Institute, Jena, Germany.

© 2023 Culemann et al. This article is distributed under the terms of an Attribution–Noncommercial–Share Alike–No Mirror Sites license for the first six months after the publication date (see <http://www.rupress.org/terms/>). After six months it is available under a Creative Commons License (Attribution–Noncommercial–Share Alike 4.0 International license, as described at <https://creativecommons.org/licenses/by-nc-sa/4.0/>).

2018; Richards et al., 1999; Summan et al., 2006; van Rooijen et al., 1996).

In an effort to revisit the specificity of Clo-Lip-mediated effects on the MoPh system, we compared the effect of Clo-Lip-mediated depletion of MoPh with the phenotypes resulting from genetic MoPh deficiency and depletion during the mouse model of K/BxN serum transfer arthritis (STA). The resulting data show that *in vivo* effects of Clo-Lip did not rely on the presence of MoPh and corresponded neither to a global nor a subset-specific deficiency in monocytes or macrophages. Instead, we observed that Clo-Lip were also readily taken up by polymorphonuclear neutrophils (PMN), which did not result in the depletion of PMN but provoked a substantial impairment of PMN function. This included a Clo-Lip-mediated block of PMN phagocytic capacity, cytokine expression, ROS production, as well as the formation of neutrophil extracellular traps (NETs) and additionally altered the migratory and swarming behavior of these cells. Depletion of PMN, in turn, resulted in a phenotype that resembled Clo-Lip treatment, and adoptive transfer of PMN, but not of MoPh, reversed the anti-inflammatory effects observed upon Clo-Lip treatment. Together, these data demonstrate that functional stunning of PMN is a major consequence of the application of Clo-Lip, whereas depletion of MoPh does not account for the anti-inflammatory effects of this widely used compound, a finding that necessitates a critical revision of the current literature on monocytes and macrophages.

Results and discussion

In an effort to validate the specificity of the action of Clo-Lip on MoPh, we decided to study the model of STA as an established mouse model mimicking the autoantibody-mediated inflammatory effector phase of RA. Monocytes, macrophages, and PMN have all been implicated in the onset and perpetuation of inflammation as well as the pathogenesis of both RA and STA (Bruhns et al., 2003; Firestein and McInnes, 2017; Knab et al., 2022; Kurowska-Stolarska and Alivernini, 2017; Solomon et al., 2005; Udalova et al., 2016; Wipke and Allen, 2001). However, the individual experimental approaches of previous studies investigating the contribution of MoPh during this and other inflammatory disease models substantially varied and often yielded discrepant results describing both a pro- and anti-inflammatory role of different subsets of MoPh (Knab et al., 2022; Kurowska-Stolarska and Alivernini, 2017).

As expected, we observed an efficient and rapid depletion of circulating CD115⁺CD11b⁺ monocytes upon *i.v.* injection of Clo-Lip into mice (Fig. 1 A and Fig. S1, A and B). The number of other leukocyte subsets within the peripheral blood including PMN, eosinophils, T cells, and B cells did not significantly change upon Clo-Lip treatment (Fig. 1 A and Fig. S1, A and B). In accordance with previously published data (Misharin et al., 2014), a single injection of Clo-Lip not only led to the disappearance of blood monocytes but also to almost complete inhibition of arthritis in the model of STA (Fig. 1 B).

Such potent anti-inflammatory effects of Clo-Lip have been previously attributed to the depletion of Ly6C^{low} monocytes and monocyte-derived macrophages, suggesting a major pro-

inflammatory role of MoPh during the onset of joint inflammation (Misharin et al., 2014; Richards et al., 1999; Solomon et al., 2005). We subsequently studied STA in various genetic models that either lacked individual monocyte and macrophage subsets or allowed their specific depletion. Initially, we decided to study NR4a1^{-/-} mice that specifically lack the Ly6C^{low} monocyte subset (Fig. 1 C; Carlin et al., 2013; Hanna et al., 2011). Notably, NR4a1^{-/-} mice showed no reduction in joint inflammation suggesting that Ly6C^{low} monocytes are dispensable for the onset of STA (Fig. 1 D). Next, we studied mice that expressed a Cre recombinase under the Cx3cr1 promoter together with a Cre-inducible diphtheria toxin (DT) receptor (Cx3cr1cre;iDTR mice). Cx3cr1 is broadly and specifically expressed by blood monocytes as well as by the pre- and perinatal precursors of all TRMs (Yona et al., 2013). Continuous injection of DT accordingly resulted in a global depletion of blood monocytes and tissue macrophages in Cx3cr1cre;iDTR mice (Culemann et al., 2019b; Fig. 1, E, F, and I). However, we again observed a regular onset of STA during these experiments (Fig. 1 G). These results substantially questioned a major proinflammatory role of MoPh during the initiation of STA as well as the MoPh specificity of Clo-Lip. Selective application of DT on days 5 and 6 prior to induction of STA, in turn, allowed the specific depletion of TRM during STA in Cx3cr1cre;iDTR mice as blood monocytes rapidly repopulated within 48 h and were thus present prior to the onset of inflammation (Fig. 1, H and I). In contrast to the phenotype observed after Clo-Lip injection, this protocol resulted in an exacerbated course of joint inflammation during STA (Fig. 1 J), which was in accordance with the reported anti-inflammatory role of Cx3cr1⁺Trem2⁺ TRMs of the synovial tissue (Alivernini et al., 2020; Culemann et al., 2019b; Friščić et al., 2021). Experiments using the mouse model of monosodium urate crystal (MSU)-induced gouty arthritis recapitulated these findings. The onset of MSU-induced arthritis was blocked by Clo-Lip injection, whereas neither the deficiency of Ly6C^{low} monocytes in NR4a1^{-/-} mice nor depletion of the MoPh compartment in DT-treated Cx3cr1cre;iDTR mice resulted in amelioration of arthritis (Fig. S1, C-F).

These data showed that using different arthritis models, the phenotype resulting from injection of Clo-Lip did not match the phenotypes resulting from a global or subset-specific deficiency of monocytes and/or macrophages. Consequently, we determined whether the observed anti-inflammatory effects of Clo-Lip indeed required the presence of MoPh or whether Clo-Lip exerted their anti-inflammatory effects independently of monocytes and macrophages. Therefore, we repeated the continuous and global depletion of MoPh by repetitive injection of DT in Cx3cr1cre;iDTR mice and additionally treated these mice with Clo-Lip or PBS, respectively (Fig. 2 A and Fig. S2 A). Notably, the Clo-Lip-induced anti-inflammatory effects fully persisted also in the absence of MoPh, where injection of Clo-Lip exerted strong and comparable anti-inflammatory effects in both DT-treated Cx3cr1cre;iDTR mice and DT-treated control mice (Fig. 2 B).

As these experiments clearly demonstrated that the anti-inflammatory effects of Clo-Lip did not rely on the depletion of MoPh, we investigated additional effects of Clo-Lip that might account for their potent anti-inflammatory properties.

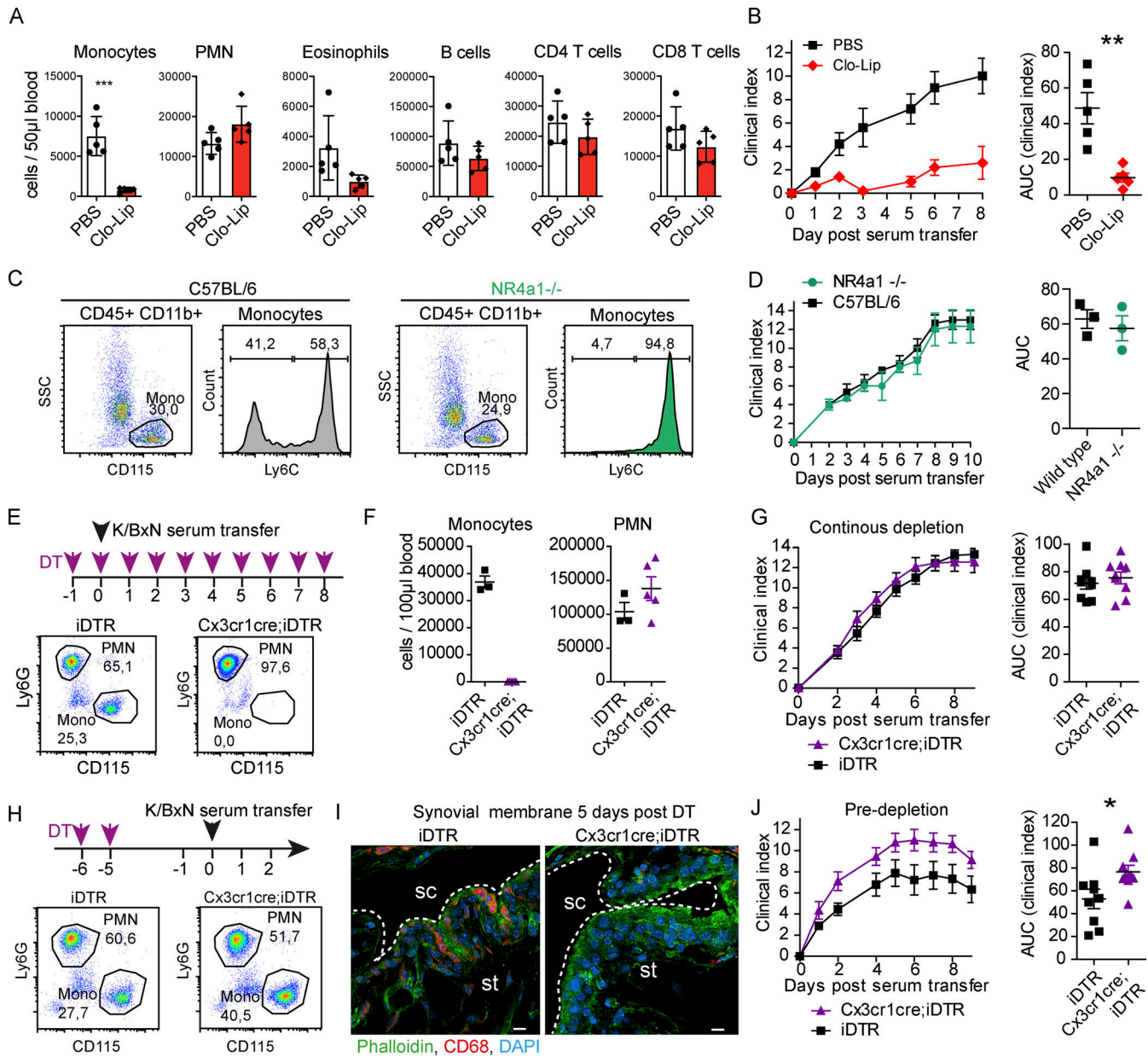


Figure 1. Joint inflammation is differentially affected by Clo-Lip and genetic deficiencies in MoPh. (A) Quantification of the number of indicated cells in 50 µl mouse blood 24 h after i.v. injection of Clo-Lip or PBS ($n = 5$ per group). Data are mean \pm SD; two-tailed Student's t test; ***, $P = 0.0003$. (B) Clinical evaluation of K/BxN STA in C57BL/6 mice treated with 200 µl Clo-Lip or PBS 24 h before arthritis induction using a semiquantitative clinical index and the corresponding area under the curve (AUC); ***, $P = 0.0027$. The experiment was performed twice. (C) Flow cytometry of CD45⁺CD11b⁺CD115⁺ monocytes in the peripheral blood of NR4a1^{-/-} and C57BL/6 wild-type mice demonstrating the absence of the CD45⁺CD11b⁺CD115⁺ Ly6C^{low} monocyte subset in NR4a1^{-/-} mice. Numbers in the flow plot correspond to the percentage of the parent population. (D) Clinical development of STA in NR4a1^{-/-} and C57BL/6 wild-type mice quantified by a semiquantitative clinical index and the corresponding AUC ($n = 3$ per group). (E) Treatment regimen for continuous monocyte and macrophage depletion of Cx3cr1cre;iDTR mice or iDTR control mice. Bottom: Representative flow cytometry plots demonstrating the depletion of blood monocytes 1 d after intraperitoneal injection of 500 ng DT. During STA, mice were treated daily starting 1 d before arthritis induction. (F) Quantification of neutrophil and monocyte numbers in 100 µl blood of Cx3cr1cre;iDTR mice ($n = 5$) and iDTR control mice ($n = 3$) 1 d after first DT injection. (G) Clinical course of STA in Cx3cr1cre;iDTR ($n = 9$) and iDTR control mice ($n = 8$) upon daily treatment with DT quantified by a semiquantitative index and the corresponding AUC. (H) Treatment regimen for predepletion of synovial macrophages of Cx3cr1cre;iDTR or iDTR control mice and representative flow cytometry plots demonstrating recovery of blood monocytes 5 d after two intraperitoneal injections of 500 ng DT. (I) Representative images of confocal laser scanning fluorescence microscopy of the synovial membrane of knee joints of Cx3cr1cre;iDTR mice or iDTR control mice 5 d after DT administration showing depletion of CD68⁺ (red) synovial macrophages in Cx3cr1cre;iDTR mice (scale bar, 10 µm). sc, synovial cavity; st, synovial tissue. (J) Clinical course of STA in predepleted Cx3cr1cre;iDTR ($n = 8$) and iDTR control mice ($n = 9$) quantified by the clinical index and the corresponding AUC. Data are mean \pm SEM; two-tailed Student's t test of AUC; *, $P = 0.0142$. Experiments (A–J) were performed at least two times. Numbers in flow plots correspond to percentages of parent population (C, E, and H).

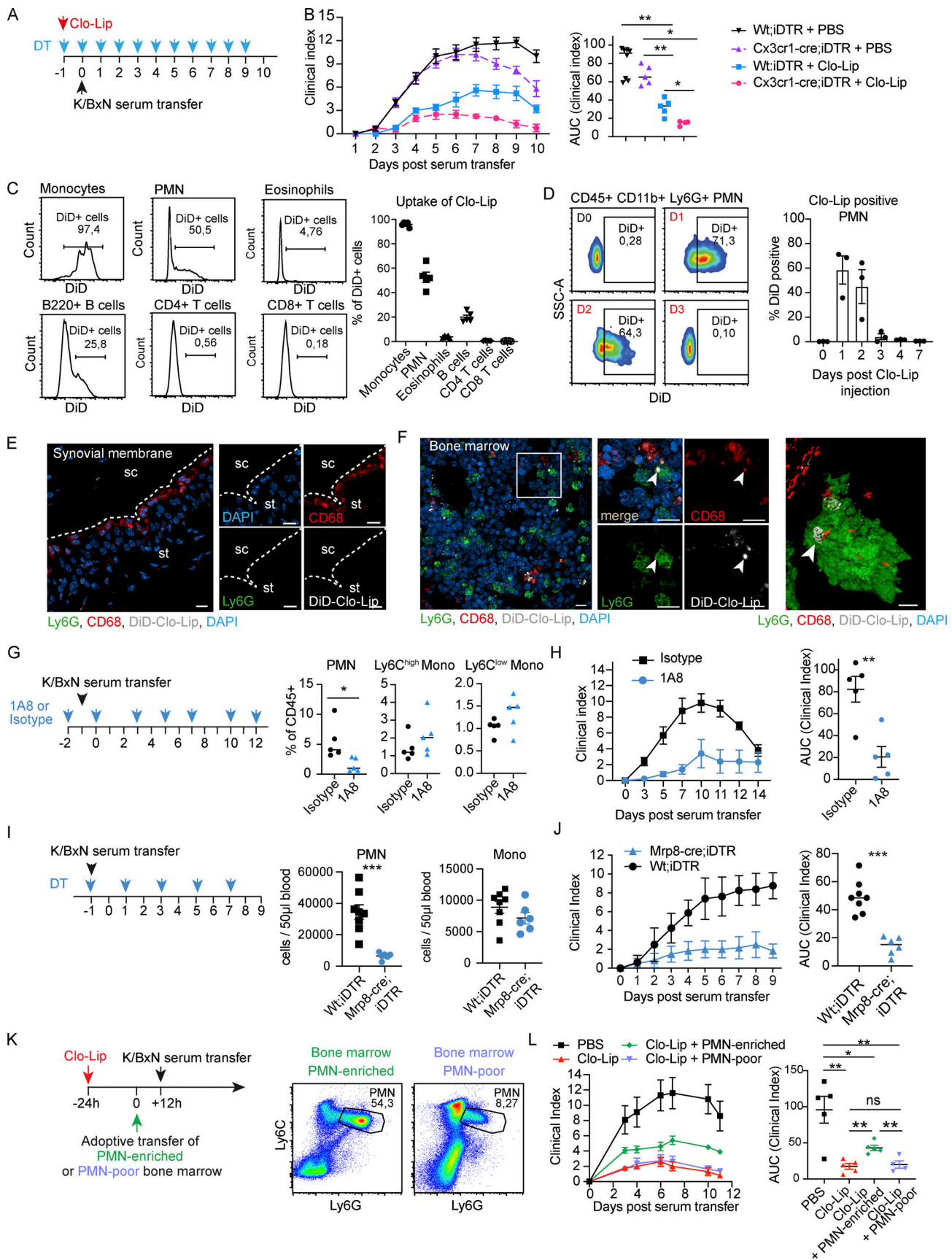


Figure 2. **Clo-Lip act independently of MoPh and are readily ingested by PMN.** (A and B) Treatment regimen (A) and clinical course (B) of K/BxN STA upon continuous monocyte and macrophage depletion in Cx3cr1cre;iDTR or iDTR control mice that were treated with 200 µl Clo-Lip or PBS 1 d before STA induction.

For MoPh depletion, mice were treated daily with DT starting 1 d before arthritis induction. **(B)** STA severity was quantified using a semiquantitative index and the corresponding AUC. Cx3cr1cre;iDTR mice + PBS ($n = 5$); iDTR control + PBS ($n = 8$); Cx3cr1cre;iDTR mice + Clo-Lip ($n = 4$); iDTR control + Clo-Lip ($n = 5$). Mann–Whitney test of AUC; *, $P < 0.05$; **, $P < 0.01$. **(C)** Flow cytometry analysis of blood of C57BL/6 mice ($n = 5$) 24 h after injection of DiD-labeled Clo-Lip, demonstrating the uptake of Clo-Lip by indicated cell types. **(D)** Uptake of DiD-labeled Clo-Lip by PMN at indicated time points. Flow plots (left) and bar graph (right) show uptake of DiD-labeled Clo-Lip by CD45⁺, CD11b⁺ Ly6G⁺ PMN before injection (D0) and after application at day 1 (D1), day 2 (D2), and day 3 (D3). Bar graph (right) shows frequencies of PMN positive for Clo-Lip ($n = 3$ mice) at indicated time points after injection. **(E and F)** Representative images of confocal laser scanning fluorescence microscopy of the synovial membrane of a knee joint (E) and bone marrow (F, left) of the femur of C57BL/6 mice 24 h after injection of DiD-labeled Clo-Lip showing the uptake of Clo-Lip (DiD, white) by macrophages (CD68, red) and PMN (Ly6G, green) in bone marrow but not in synovial tissue. sc, synovial cavity; st, synovial tissue. Scale bars: 10 μm . **(F)** Right: 3D reconstruction of a bone marrow PMN (Ly6G, green) that ingested DiD-labeled Clo-Lip (white) and macrophage debris (CD68, red). Scale bar: 2 μm . **(G)** Treatment regimen for antibody (1A8 or isotype)-mediated PMN depletion (left) and quantification of blood PMN and blood monocytes 1 d after first antibody injection (right); $n = 5$ mice per group; two-tailed Student's t test; *, $P = 0.0277$. **(H)** Clinical course of STA (clinical index as mean \pm SD) induced in mice treated with PMN-depleting antibody (1A8) or isotype control ($n = 5$ per group) and the corresponding AUC of the clinical index. Data are mean \pm SEM; two-tailed Student's t test of AUC; **, $P = 0.0035$. **(I)** Treatment regimen for PMN depletion in Mrp8-cre;iDTR mice (left) and cell counts of PMN and monocytes in blood 1 d after first DT injection (right); Wt;iDTR: $n = 8$ mice and Mrp8-cre;iDTR $n = 6$ mice. Data are mean \pm SEM; two-tailed Student's t test; **, $P = 0.0003$. **(J)** Clinical course of STA (clinical index as mean \pm SD) in DT-treated Mrp8-cre;iDTR mice ($n = 6$ mice) or iDTR control mice ($n = 8$ mice) and the corresponding AUC of the clinical index. Mann–Whitney test of AUC; ***, $P = 0.0007$. **(K)** Treatment strategy (left) testing the effect of adoptive transfer of PMN-enriched or PMN-poor bone marrow cells in mice 24 h after Clo-Lip injection. STA was induced 12 h after adoptive transfer. Flow plots (right) show cellular composition of PMN-enriched and PMN-poor bone marrow cell suspension used for adoptive transfer. 5×10^6 PMN-enriched or PMN-poor bone marrow cells were i.v. injected. **(L)** Clinical course and AUC of STA in mice treated with Clo-Lip or PBS upon receiving PMN-enriched or PMN-poor bone marrow. PBS: $n = 5$ mice; Clo-Lip: $n = 5$ mice; Clo-Lip + PMN-enriched: $n = 5$ mice; Clo-Lip + PMN-poor: $n = 4$ mice. Data are mean \pm SEM; two-tailed Student's t test of AUC; *, $P < 0.05$; **, $P < 0.01$. Experiments in A, B, and G–J were performed once and were performed at least two times in C–F, K, and L. Numbers in flow cytometry plots in C, D, and K correspond to percentages of parent population.

Therefore, we studied the uptake of i.v.-injected liposomes into alternative leukocyte subsets. While Vybrant DiD-labeled PBS liposomes were only taken up by blood monocytes (Fig. S2 B), we observed that DiD-labeled Clo-Lip were taken up both by blood monocytes as well as by around 50% of circulating PMN and a smaller percentage of B cells (Fig. 2 C). In contrast to monocyte numbers, however, PMN numbers remained constant and PMN did not show signs of apoptosis such as an increased annexin V staining despite uptake of Clo-Lip (Fig. 1 A and Fig. S2 C). DiD labeling of circulating PMN by Clo-Lip persisted for 2 d before the signal within this cellular fraction disappeared (Fig. 2 D). Immunofluorescence microscopy additionally confirmed uptake of DiD-labeled Clo-Lip into macrophages and PMN of the bone marrow, whereas we did not observe uptake into synovial TRM (Fig. 2, E and F).

PMN were reported to act as essential effectors of the proinflammatory response during STA (Wipke and Allen, 2001). We accordingly confirmed that depletion of PMN by the Ly6G antibody 1A8 or alternatively by DT treatment of Mrp8cre;iDTR mice effectively blocked the onset of STA (Fig. 2, G–J; and Fig. S2, D–F). These data showed that depletion of PMN but not depletion or absence of MoPh matched the phenotype observed in response to Clo-Lip treatment. Therefore, we hypothesized that the observed uptake of Clo-Lip by PMN might impair PMN function and thereby contribute to the anti-inflammatory effects exerted by Clo-Lip in vivo. Adoptive transfer of the PMN-enriched fraction of bone marrow cells indeed abated the anti-inflammatory effects of Clo-Lip treatment during STA (Fig. 2, K and L). In contrast, the transfer of the PMN-poor fraction of bone marrow cells, which was rich in MoPh, did not impact the Clo-Lip-mediated suppression of STA (Fig. 2, K and L). Collectively, these experiments thus confirmed an essential contribution of PMN during this disease model and additionally suggested a major role of PMN during the Clo-Lip-mediated anti-inflammatory effects.

We therefore determined a potential impact of Clo-Lip uptake on PMN function in more detail. A phenotypic analysis of

PMN in Clo-Lip-treated animals indeed revealed significant changes in the expression of PMN surface markers with the downregulation of molecules such as CD11b and CD16 (Fig. 3 A). Also, the measurement of PMN-mediated intracellular ROS production showed a drastically reduced PMA-induced oxidative burst of PMN derived from Clo-Lip-treated mice (Fig. 3 B). This was paralleled by a defect of Clo-Lip-exposed PMN to form NETs (Fig. 3 C). PMN from Clo-Lip-treated animals additionally displayed a reduced secretion of proinflammatory cytokines such as TNF α and IL-6 (Fig. 3 D and Fig. S2 G), as well as a decreased phagocytic capacity, illustrated by an impaired uptake of BSA-coated beads and IgG-coated latex beads (Fig. 3, E and F). We additionally performed intravital microscopy to study the impact of Clo-Lip on the migratory behavior of PMN within inflamed tissues. Here, we assessed PMN migration in a model of TNF-induced inflammation of the microvasculature of the cremaster muscle (Fig. 3 G) and additionally studied the swarming pattern of PMN in response to laser-induced tissue damage (Lämmermann et al., 2013; Uderhardt et al., 2019) in the peritoneal cavity (Fig. 3 H). These experiments showed that PMN in Clo-Lip-treated mice displayed an altered migratory behavior with significant changes in their velocity, accumulated distance, and directionality in response to TNF (Fig. 3 G). Clo-Lip treatment likewise resulted in a substantially reduced swarming capacity, which entailed a reduced formation of PMN clusters at the site of injury (Fig. 3 H). Injection of Clo-Lip thus substantially altered the migratory behavior of PMN, an alteration previously defined as “stunning” (García-Prieto et al., 2017).

Our current data show that the widely reported anti-inflammatory effects resulting from the in vivo injection of Clo-Lip are not primarily linked to the Clo-Lip-mediated depletion of proinflammatory MoPh. Notably, Clo-Lip-induced amelioration of arthritis was evident in both wild-type and MoPh-deficient animals. Moreover, phenotypes observed during the course of STA in various MoPh-deficient animals did not resemble and even contrasted the phenotypes observed after

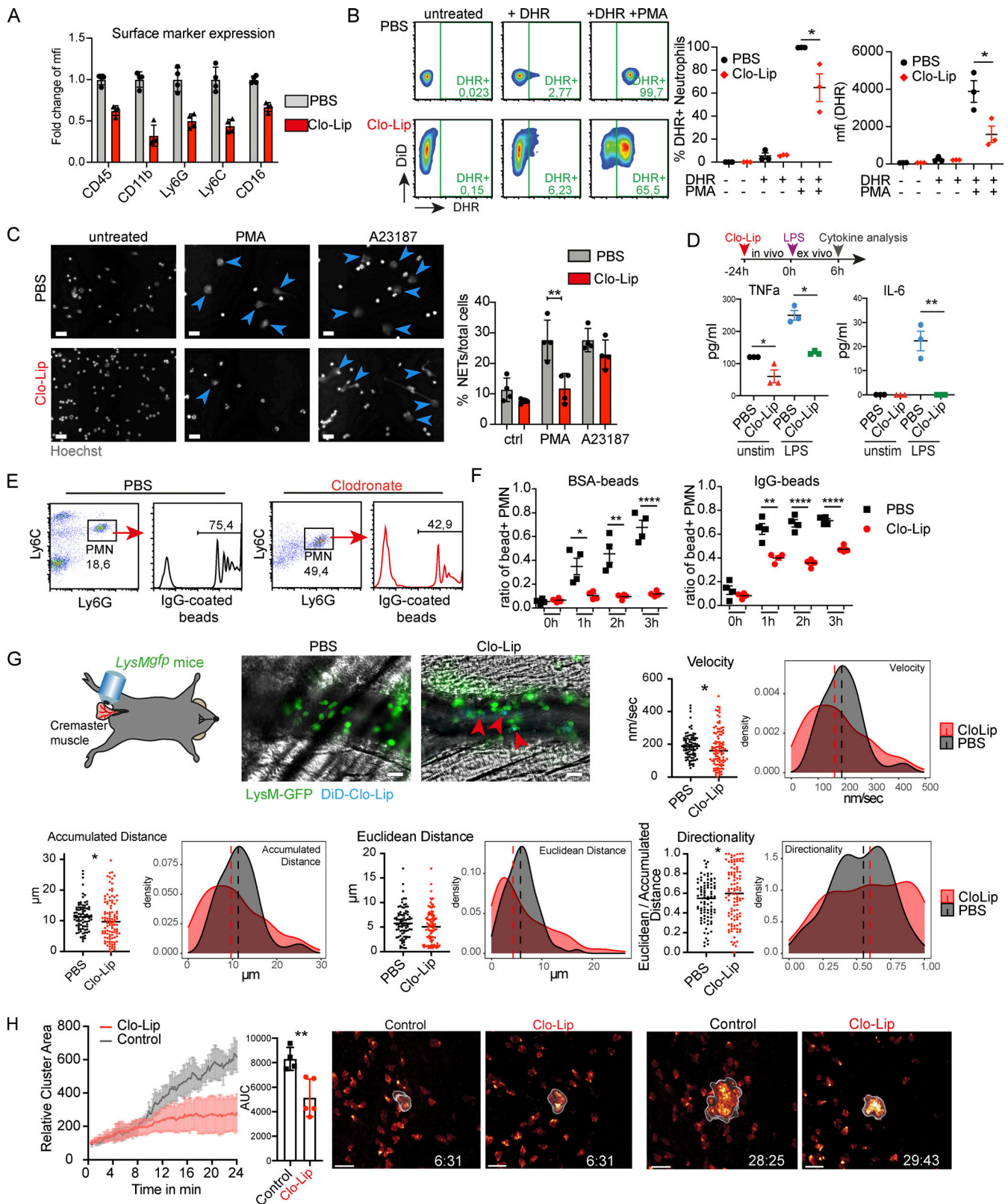


Figure 3. Uptake of Clo-Lip results in stuning of PMN. (A) Surface detection of indicated markers on blood PMN 24 h after PBS or Clo-Lip injection ($n = 4$ mice per group). (B) Production of intracellular ROS by PMN. Blood of Clo-Lip-treated ($n = 3$ mice) and PBS-treated C57BL/6 mice ($n = 3$ mice) was collected 24 h after injection. Ex vivo PMA (100 ng/ml)-stimulated and untreated blood was incubated with the ROS-indicator DHR. ROS production was quantified by measurement of the mean fluorescence intensity (mfi) of DHR. Data are mean \pm SEM; two-tailed Student's t test; *, $P < 0.05$. (C) Induction of the formation of NETs using PMA (100 ng/ml) or the calcium ionophore A23187 (2 μ g/ml). Blood of mice was collected 24 h after Clo-Lip (200 μ l, i.v.) or PBS injection. NETs (indicated by blue arrowheads in the representative figures, scale bar: 20 μ m) were quantified 2 h after ex vivo stimulation as a percentage of total cells ($n = 4$

mice per group). Data are mean \pm SD; two-tailed Student's *t* test; **, *P* = 0.0082. **(D)** Quantification of TNF α and IL-6 levels in supernatants of ex vivo stimulated PMN derived from Clo-Lip- or PBS-treated mice. Blood of C57BL/6 mice treated either with Clo-Lip (*n* = 5 mice) or PBS (*n* = 5 mice) was collected 24 h after Clo-Lip or PBS application. Blood of mice of each group was pooled, and PMN were enriched using a magnet-based enrichment kit and stimulated for 6 h with 2.5 μ g/ml LPS. **(E and F)** Phagocytic capacity of PMN from C57BL/6 mice that received either 200 μ l Clo-Lip (*n* = 4 mice) or PBS (*n* = 4 mice) 24 h before blood collection. Whole blood samples of each mouse were incubated with BSA- or IgG-coated beads for 1 h, 2 h, or 3 h. **(E)** Representative flow cytometry plots of Clo-Lip- or PBS-treated PMN incubated with IgG-beads for 3 h. **(F)** Ratio of bead⁺ PMN at indicated time points of incubation with beads. Data are mean \pm SEM; two-tailed Student's *t* test; *, *P* < 0.05; **, *P* < 0.01; ***, *P* < 0.0001. **(G)** Characterization of PMN migration using intravital microscopy. Inflammation of the cremaster muscle was induced by intrascrotal injection of 0.5 μ g TNF α into LyM^{GFP} mice. Mice (*n* = 4 per group) received 100 μ l Clo-Lip (blue) or PBS 24 h before imaging. GFP⁺ PMN (left panel: representative images of vessels containing PMN [green]; scale bar: 10 μ m) were tracked for 2 min beginning 2.5 h after injection of TNF α . Absolute values (left) and relative distribution (right) of velocity, accumulated distance, Euclidean distance, and directionality of PMN were quantified. PBS-treated: *n* = 68 PMN pooled from four mice; Clo-Lip-treated: 104 PMN pooled from four mice. Statistical differences of distributions were calculated using Kolmogorov–Smirnov test; *, *P* < 0.05. **(H)** Intravital microscopy-based quantification (left) and representative images (right) of PMN cluster formation in response to laser-induced tissue damage of the peritoneal serosa. Data are mean \pm SD; two-tailed Student's *t* test; **, *P* = 0.0084. Control mice: *n* = 4; Clo-Lip-treated mice: *n* = 5. Numbers indicated in images represent time in min. Scale bar: 30 μ m. Experiments in A and C were performed at least two times. Experiments in B and D–H were performed once.

Clo-Lip injection. The absence of PMN, in turn, exactly matched the Clo-Lip-induced STA phenotype, and adoptive transfer of PMN, but not of MoPh, reversed the anti-inflammatory effects of Clo-Lip treatment in vivo. Although injection of Clo-Lip did not change PMN numbers, we observed uptake of Clo-Lip by PMN, which substantially altered PMN function and resulted in a stunned PMN phenotype. Such Clo-Lip-exposed PMN were characterized by an altered migratory and swarming behavior, a defective oxidative burst, impaired NET formation, and reduced cytokine expression as well as a limited phagocytic capacity, all effects that might explain the potent anti-inflammatory effects of Clo-Lip in vivo. The exact molecular mechanism by which Clo-Lip alter PMN function remains unclear at this stage, but its identification might yield attractive targets for future anti-inflammatory therapies. It remains equally unclear why PMN accumulated DiD in response to DiD-labeled Clo-Lip, but not after labeling with DiD-labeled PBS liposomes. A potential explanation is an impaired degradation of DiD in Clo-Lip-exposed PMN.

Our findings likely explain many of the previously observed discrepancies that have emerged in the field of monocyte and macrophage research. Notably, many of the previous studies investigating the role of MoPh during inflammation heavily relied on the use of Clo-Lip, where this approach was considered to specifically deplete MoPh. As Clo-Lip reproducibly exerts a potent anti-inflammatory effect in many inflammatory settings, such studies often provoked the conclusion that monocytes and macrophages primarily act as proinflammatory effector cells and substantially promote inflammation and inflammation-associated tissue damage (Kurowska-Stolarska and Alivernini, 2017; Moreno, 2018; Richards et al., 1999; Solomon et al., 2005). Our current data, in turn, indicate that many of the observed anti-inflammatory effects are not primarily linked to a depletion of MoPh, but can be instead attributed to a Clo-Lip-mediated block of PMN function. Both genetic and pharmacologic data consistently support a scenario where PMN act as primary effectors of the acute inflammatory response.

The role of MoPh during inflammation, in turn, is much more disputed. Theoretically, MoPh might exert both pro- and anti-inflammatory functions. However, increasing data, which are based on sophisticated genetic models, single-cell sequencing, and intravital imaging, support a more straight-forward scenario

where the MoPh compartment primarily exerts anti-inflammatory and tissue-protective functions, both during the onset and the resolution of inflammation (Blériot et al., 2020). In particular, TRM seem to serve as anti-inflammatory tissue-resident guardians that provide anti-inflammatory barriers and prevent spontaneous PMN-induced inflammation (Uderhardt et al., 2019). Although our current study thus introduces another big question mark on the previously described role of MoPh during inflammation, it might offer a chance to critically revisit the contribution of these cells during homeostasis and inflammation and substantially improve our understanding of these key players of innate immunity.

Materials and methods

Animal models

The animal experiments were performed in accordance with German guidelines and laws and were approved by the local animal ethics committees of the Regierung von Mittelfranken and the Animal Care and Ethics Committee at Centro Nacional de Investigaciones Cardiovasculares (CNIC), respectively. Mice of both sexes between the ages of 8–20 wk were used for experiments. Cx3cr1cre;iDTR mice were generated by breeding C57BL/6-Gt(ROSA)26Sortm1(HBEGF)Awai/J (iDTR) purchased from Jackson Laboratory with STOCK Tg(Cx3cr1cre)MW126Gsat/Mmucd mice (Cx3cr1cre; identification number 036395-UCD) from the Mutant Mouse Regional Resource Center, a National Institutes of Health–funded strain repository, and were donated to the Mutant Mouse Regional Resource Center by the National Institute of Neurological Disorders and Stroke–funded GENSAT BAC transgenic project. NR4A1^{-/-} were obtained from the Jackson Laboratory. K/BxN STA was initiated by intraperitoneal injection of 125–150 μ l K/BxN serum collected from arthritic K/BxN mice. The clinical evaluation of arthritis development was quantified by the application of a semiquantitative clinical index. The clinical index reaching from 0 (no signs of inflammation) to 16 (maximum inflammation) is calculated as the sum of scores allocated to each paw, with 0 = no signs of inflammation, 1 = slight inflammation and reddening of the paw, 2 = moderate inflammation and erythema, 3 = severe inflammation and erythema, and 4 = maximum inflammation and erythema. MSU crystal-induced paw inflammation was induced by injection of 50 μ l (20 mg/ml) MSU crystals

into one hind paw. The contralateral paw received PBS as control. Paw swelling was measured daily using a Dial Thickness Gauge (G-1A, Peacock, OZAKI MFG, Co., Ltd.)

Liposomes

Clodronate liposomes (SKU: C-005) and PBS liposomes (SKU: P-005) were commercially available and purchased from Liposoma BV (<https://clodronateliposomes.com>, <http://clodronateliposomes.org>). The concentration of the clodronate in the suspension was 5 mg/ml. Liposome suspensions were injected directly without any further dilutions. For labeling of clodronate liposomes with Vybrant DiD (Vybrant DiD Cell-Labeling Solution, Invitrogen, V22887), 10 μ l of the Vybrant dye solution was added to 1 ml clodronate liposome suspension and mixed by gentle shaking. After incubation at 37°C for 20 min (slowly shaking), labeled liposome suspension was centrifuged at 1,500 rpm for 5 min, producing a loose phase of liposomes and an upper aqueous phase. The aqueous phase was removed, and an equivalent volume of PBS was added to the liposomes and mixed well by gentle pipetting. After an additional centrifugation step (1,500 rpm, 5 min) and removal of the upper aqueous phase, an equivalent volume of PBS was added to liposomes to get the original volume.

Cellular depletion approaches

For DT-mediated cell depletion in Cx3cr1cre;DTR mice, DT (500 ng/mouse) was either injected twice within 24 h starting 6 d before arthritis induction for the predepletion or daily (500 ng DT/mouse on the first day, and 100 ng DT/mouse on following days) starting 1 d before arthritis induction for continuous depletion.

Clo-Lip (200 μ l) were i.v. injected. For imaging and flow cytometry, liposomes were labeled with Vybrant DiD using Vybrant Cell-Labeling solutions. 10 μ l of Vybrant dye per ml liposomes was incubated for 20 min at 37°C slowly shaking followed by two washing steps with PBS and reconstitution to the original volume. Arthritis induction, intravital microscopy (IVM), and blood collection for ex vivo stimulation of neutrophils were conducted 24 h after liposome injection.

Antibody-mediated depletion was performed by intraperitoneal injection of 500 μ g InVivoMab anti-mouse Ly6G antibody (1A8, BioXCell) every 2 d. Isotype injection was used as a control.

Adoptive transfer experiments

Bone marrow of C57BL/6 mice was processed to generate a PMN-enriched fraction and a PMN-poor fraction. Bone marrow of femur and tibia was flushed and filtered (70 μ m). Fractionation of bone marrow cells was achieved by using a Histopaque gradient (bottom layer: 3 ml Histopaque 1119 [11191-100ML; Sigma-Aldrich]; middle layer: 3 ml Histopaque 1077 [10771-100ML; Sigma-Aldrich]; top layer: 5 ml bone marrow suspension), and centrifugation at room temperature, 800 *g* for 40 min. PMN were harvested from the interface of Histopaque 1077 and 1119. The PMN-poor fraction was further purged from PMN two times by using MACS cell separation columns and Anti-Ly6G MicroBeads UltraPure, mouse (Miltenyi). 5 \times 10⁶ PMN-enriched or PMN-poor bone marrow cells were i.v. injected.

Flow cytometry

Blood samples (50 to 100 μ l) were collected in heparin- or EDTA-containing tubes and transferred into PBS with 4% FCS and 2 mM EDTA. Erythrocyte lysis was performed with ddH₂O followed by reconstitution with 10 \times PBS. Cells were blocked with 30 μ l PBS containing 10% rat serum and 1% FcBlock for 10 min at room temperature followed by supplementation of PBS containing antibodies to a final volume of 80 μ l and incubation at 4°C for 20 min. After washing, cells were taken up in PBS with 4% FCS and 2 mM EDTA for flow cytometry with a CytoFLEX S (Beckman Coulter). For the preparation of hind paws for flow cytometry, skin, muscle, and tendons of hind paws were removed. Tissue was dissociated in digestion medium containing RPMI, 10% heat-inactivated FCS, collagenase (2 mg/ml) from *Clostridium histolyticum* (Sigma-Aldrich), and 0.03 mg/ml DNase I from bovine pancreas (Sigma-Aldrich) for 45 min at 37°C in a shaking incubator. After washing with PBS containing 2% FCS and 2 mM EDTA, cell suspension was filtered (70 μ m filter), blocked (PBS with 10% rat serum), and stained with fluorophore-conjugated antibodies. The following antibodies were used in this study: CD45.2-Alexa Flour 700 (cat#: 109822, lot: B202497, clone: 104, dilution: 1:500; BioLegend), CD11b-PE/Cy7 (cat#: 101216, lot: B185646, clone: M1/70, dilution: 1:500; BioLegend), Ly6G-Alexa Fluor 488 (cat#: 127626, lot: B240194, clone: 1A8, dilution: 1:400; BioLegend), Ly6G-PerCP/Cy5.5 (cat#: 127616, clone: 1A8, dilution: 1:400; BioLegend), and CD115-BV421 (cat#: 135513, clone: AFS98, dilution: 1:500; BioLegend). Ly6G-Alexa Flour 488 (cat#: 128022, lot: B248739, clone: HK1.4, dilution: 1:400; BioLegend), Ly6G-Alexa Fluor 647 (cat#: 127610, lot: B204928, clone: 1A8, dilution: 1:200; BioLegend), Ly6G-Brilliant Violet 421 (cat#: 127627, lot: B193096, clone: 1A8, dilution: 1:400; BioLegend), CD4-FITC (cat#: 100406, clone: GK1.5, dilution: 1:400; BioLegend), and B220-Pacific Blue (cat#: 103227, clone: RA3-6B2, dilution: 1:400; BioLegend). Kaluza (Beckman Coulter, v.1.5a) and CytExpert (Beckman Coulter, v.2.2.0.97) or FlowJo (v.7.6.5) were used for data analysis.

Ex vivo characterization of PMN

Quantification of ROS generation was performed by incubating whole blood cells with either dihydrorhodamine-123 (DHR; 3 μ g/ml; Molecular Probes) or DHR together with PMA (100 ng/ml) for 30 min at 37°C. After treatment, erythrocytes were lysed with ddH₂O. Staining of cells with fluorophore-conjugated antibodies and analysis was performed as described above for flow cytometry. For quantification of the phagocytic capacities of PMN, blood was collected 24 h after injection of Clo-Lip or PBS and incubated either with IgG-coated beads or BSA-coated beads. Beads (Fluoresbrite YG Carboxylate Microspheres, 1 μ m; Polyscience) were sonicated for 5 min and coated with mouse IgG or BSA (2 mg/ml) in 50 mM MES/2 mM 1-ethyl-3-(3-dimethylaminopropyl)carbodiimide (pH 6.1) for 12 h at room temperature. After washing, the beads were resuspended in PBS. Cells were incubated with the beads for 1, 2, or 3 h at 37°C. The uptake of beads was quantified by flow cytometry. Quantification of NET formation was performed by treating blood cells with either PMA (100 ng/ml), A23187 (2 μ g/ml), or PBS as a control.

Prior to *ex vivo* induction of NET formation, mice received 200 μ l Clo-Lip (*i.v.*) or PBS as control, and blood was collected 24 h later in EDTA-containing tubes. Erythrocytes were lysed in ddH₂O and samples were reconstituted with 10 \times PBS. Cells were transferred onto a glass chamber slide (150,000 cells/well) and incubated for 3 h at 37°C with the aforementioned stimuli. After fixation of cells using 4% paraformaldehyde for 20 min, the cells were washed three times with PBS and blocked with 10% FCS/2% BSA in PBS at room temperature for 1 h. After washing, samples were incubated with Hoechst 33342 for 90 min at room temperature. After washing with PBS and water, the samples were mounted with DAKO mounting medium. NET formation was defined as Hoechst⁺ events, which had at least a fivefold mean nuclear size. For cytokine measurements after *ex vivo* stimulation, C57BL/6 mice received 200 μ l Clo-Lip or PBS 24 h before blood sampling. PMN of blood were enriched using the EasySep Mouse Neutrophil Enrichment Kit. 1.5 \times 10⁵ cells in 200 μ l per well (96-well format) were stimulated with 2.5 μ g/ml LPS for 6 h. Cytokines were quantified using Mouse IL-6 DuoSet ELISA (DY406; R&D Systems) and Mouse TNF- α DuoSet ELISA (DY410; R&D Systems).

Immunofluorescence and IVM

For immunofluorescence microscopy, femur and tibia with intact knee joint were incubated in 4% paraformaldehyde overnight at 4°C for fixation. Tissue was decalcified in PBS containing 14% EDTA (pH adjusted to 7.2 with NaOH) for 10 d at 4°C. After decalcification, tissue was incubated in 30% sucrose for 24 h at 4°C, embedded into TissueTek, and stored at -80°C. Sections of 7 μ m were generated with a Leica CM 3050 S cryostat and Cryofilm Type 2C (9; C-MK001-A2; Section Laboratory). Sections were blocked with PBS/10% rat serum for 1 h and stained with fluorophore-conjugated antibodies in PBS/5% rat serum overnight at 4°C. After staining, the sections were washed with PBS and stained with DAPI (1 μ g/ml in PBS) for 10 min. Following a final washing step, the sections were mounted using Dako Fluorescence Mounting Medium. The following antibodies were used for staining: Ly6G-Alexa Fluor 488 (cat#: 127626, lot: B240194, clone: 1A8, dilution: 1:400; BioLegend) and CD68-Alexa Fluor 594 (cat#: 137020, lot: B239125, clone: FA-11, dilution: 1:400; BioLegend). Confocal laser scanning fluorescence microscopy was conducted with a Leica TCS SP 5 II confocal microscope equipped with an acousto-optic tunable filter and acousto-optical beam splitter, and a hybrid detector (HyD) on a DMI6000 CS frame. An HCX PL APO 100 \times oil objective with a numerical aperture of 1.44 was used. Sequential scans generated fluorescence signals using an argon laser at 488 nm detecting AlexaFluor488 with a HyD detector at 500–550 nm, a helium–neon laser at 633 nm to detect DiD and Alexa Fluor 647 with a HyD detector at 650–700 nm, a diode-pumped solid-state laser at 561 nm for detection of Alexa Fluor 594 with a HyD at 600–650 nm, and a 458 nm argon laser for detection of DAPI with a HyD at 470–520 nm. Deconvolution was performed using Huygens Professional. Imaris software was used to generate 3D reconstructions.

IVM

IVM of the cremaster model was performed as described before. Briefly, for IVM, 6 to 12-wk-old LysM^{GFp} mice received 0.5 μ g

TNF α (R&D Systems) intrascrotally to induce inflammation. 150–210 min after TNF α injection, cells were tracked for 2 min using a 3i (Intelligent Imaging Innovations) microscopy system with Axio Examiner Z.1 work station (Zeiss) and a 3-Dimensional Motorized Stage (Sutter Instrument). The equipment of the microscope included a CoolLED pE widefield fluorescence LED light source system (CoolLED Ltd. UK) and a quad pass filter cube with Semrock Di01-R405/488/561/635 dichroic and FF01-446/523/600/677 emitter. Using a Plan-Apochromat 40 \times W NA 1.0 ∞ /0 objective (Zeiss), images were acquired with a CoolSnap HQ2 camera (6.45 \times 6.45- μ m pixels, 1,392 \times 1,040 pixel format; Photometrics). The SlideBook software (Intelligent Imaging Innovations) was used for image acquisition. For intravital microscopy of the peritoneal serosa, C57BL/6 (Jackson Laboratory) between ages 10 and 18 wk were used. Mice received 100 μ l Clo-Lip or control liposomes via *i.v.* injection 24 h before intravital imaging experiments. 0.3 μ g of the chemoattractant MIP-2 (cat#: 250-15; Peprotech; recombinant murine MIP-2) was used topically to pre-*elicit* neutrophils into the parietal peritoneal serosa for 2 h so that they were present at the time the stromal lesion was initiated. Neutrophils were labeled *in situ* using 1.5 μ g purified Gr-1 FITC (clone: RB6-8C5, cat#: 108405; BioLegend). Purification of the antibody was performed using 10 kD centrifugal filters (Ultracel-10K; cat#: UFC501024; Millipore; Amicon) to remove BSA and sodium azide from the antibody solution. Intravital imaging was done as previously (Uderhardt *et al.*, 2019) described with slight modifications. Imaging was performed on a Zeiss LSM 880 NLO two-photon microscope equipped with a 20 \times water immersion objective (cat#: 421452-9880-000; Zeiss; W Plan-Apochromat 20 \times /1.0 DIC D = 0.17 M27 75 mm). Animals were anesthetized with isoflurane (cat#: 1214; CP Pharma). The animal was shaved, and a midline incision was made into the abdominal wall. Subsequently, another incision into the peritoneal wall was made along the linea alba to expose the peritoneal serosa. The peritoneal wall was carefully retained using two small sutures (Ethicon; coated VICRYL-polyglactin 6/0; cat#: V134H) and mounted on a 12 \times 25 mm plastic base plate with a raised 12 mm circular plate using Vetbond (3M; cat#: 1469SB). 10 μ l of sterile prewarmed HBSS buffer with Ca⁺ and Mg⁺ (cat#: 14025-050; Gibco), containing MIP-2 and Gr1-FITC, was applied onto the surface, before covering the serosa with a sterilized cover glass (cat#: 4663433; Paul Marienfeld). The animal was then transferred to the heated microscopic imaging chamber. The serosa was kept at a temperature of 36°C using an adjustable heater (WPI; Air-Therm SMT). Animals that showed signs of surgical damage or bleeding were not studied further. Data were acquired at a resolution of 512 \times 512 (12 bit) in stacks of 12 frames each 3 μ m apart at a frame rate of 943.72 ms and a zoom of 1.0 using ZEN software (Zen 2.1 SP3; Zeiss). Sterile tissue damage was induced using laser pulses at 800 nm to produce lesions (10 \times zoom with 20 \times objective) with a damage diameter of 20–30 μ m. The lesion can be identified as an autofluorescence signal in the imaging channels, which can be recorded over time. For imaging, the laser was tuned to 930 nm and the following filter cubes were used: SP 485; BP 500-550; BP 575-610. Raw imaging data were processed and analyzed with Imaris 9.5.1 (Bitplane). Neutrophil

dynamics were recorded immediately after the laser pulse for 30 min. To assess relative cluster growth, a three-dimensional iso-surface of Gr-1 intensity was constructed around the lesion using the Imaris surface generation tool with default settings. Cluster area was extracted over time and normalized to time zero.

Online supplementary material

Fig. S1 shows gating strategies and data from the model of MSU-induced gouty arthritis. **Fig. S2** provides additional gating strategies for identifying leucocyte subsets in mice upon DT-induced deletion of MoPh, upon DiD labeling, after annexin V staining, as well as upon antibody or DT-induced PMN depletion.

Acknowledgments

We thank A. Klej, Rita Weinkam, and R. Palmisano, as well as the Optical Imaging Center Erlangen for excellent technical assistance.

This work was supported by the Deutsche Forschungsgemeinschaft (FG 2886 “PANDORA” – B01/B02/A03/B04 to G. Krönke, F. Nimmerjahn, G. Schett, and M.H. Hoffmann, respectively, and the CRC1181-A03/A01/A02/A07/C03 Z2 to G. Krönke, G. Schett, F. Nimmerjahn, and M.H. Hoffmann), the Emerging Field Initiative of the Friedrich-Alexander University Erlangen-Nürnberg (EFI_Verbund_Med_05_MIRACLE to G. Krönke), the Bundesministerium für Bildung und Forschung (MASCARA to G. Krönke and G. Schett; MelAutim to G. Krönke), and the European Union (Horizon 2020 ERC-2014-StG 640087 – SOS and ERC-2020-CoG 101001866 – INSPIRE to G. Krönke; and ERC-2018-SyG nanoSCOPE and RTCure to G. Schett). This work was supported by grants R01AI165661 from the National Institutes of Health/National Institute of Allergy and Infectious Diseases, H2020-FET-OPEN-2018-2020 (no. 861878) from the European Commission to A. Hidalgo and M.H. Hoffmann, and HR17_00527 from Fundacion La Caixa to A. Hidalgo. The CNIC is supported by the Ministerio de Ciencia e Innovacion and the Pro-CNIC Foundation and is a Severo Ochoa Center of Excellence (MICINN award CEX2020-001041-S).

Author contributions: S. Culemann designed the study, performed experiments, interpreted results, and wrote the manuscript. K. Knab, M. Euler, A. Wegner, H. Garibagaoglu, J. Ackermann, S. Uderhardt, K. Fischer, D. Kienhöfer, G. Crainiciuc, J. Hahn, and A. Grüneboom performed experiments, collected data, and interpreted results. F. Nimmerjahn, A. Hidalgo, and G. Schett provided expertise, interpreted data, and wrote the manuscript. M.H. Hoffmann and G. Krönke designed the study and experiments and wrote the manuscript. All authors read and commented on the manuscript.

Disclosures: The authors declare no competing interests exist.

Submitted: 23 March 2022

Revised: 4 January 2023

Accepted: 6 March 2023

References

- Alivernini, S., L. MacDonald, A. Elmesmari, S. Finlay, B. Tolusso, M.R. Gigante, L. Petricca, C. Di Mario, L. Bui, S. Perniola, et al. 2020. Distinct synovial tissue macrophage subsets regulate inflammation and remission in rheumatoid arthritis. *Nat. Med.* 26:1295–1306. <https://doi.org/10.1038/s41591-020-0939-8>
- Barrera, P., A. Blom, P.L. van Lent, L. van Bloois, J.H. Beijnen, N. van Rooijen, M.C. de Waal Malefijt, L.B. van de Putte, G. Storm, and W.B. van den Berg. 2000. Synovial macrophage depletion with clodronate-containing liposomes in rheumatoid arthritis. *Arthritis Rheum.* 43:1951–1959. [https://doi.org/10.1002/1529-0131\(200009\)43:9<1951::AID-ANR5>3.0.CO;2-K](https://doi.org/10.1002/1529-0131(200009)43:9<1951::AID-ANR5>3.0.CO;2-K)
- Blériot, C., S. Chakarov, and F. Ginhoux. 2020. Determinants of resident tissue macrophage identity and function. *Immunity.* 52:957–970. <https://doi.org/10.1016/j.immuni.2020.05.014>
- Bogie, J.F., P. Stinissen, and J.J. Hendriks. 2014. Macrophage subsets and microglia in multiple sclerosis. *Acta Neuropathol.* 128:191–213. <https://doi.org/10.1007/s00401-014-1310-2>
- Bruhns, P., A. Samuelsson, J.W. Pollard, and J.V. Ravetch. 2003. Colony-stimulating factor-1-dependent macrophages are responsible for IVIG protection in antibody-induced autoimmune disease. *Immunity.* 18: 573–581. [https://doi.org/10.1016/S1074-7613\(03\)00080-3](https://doi.org/10.1016/S1074-7613(03)00080-3)
- Caër, C., and M.J. Wick. 2020. Human intestinal mononuclear phagocytes in Health and inflammatory bowel disease. *Front. Immunol.* 11:410. <https://doi.org/10.3389/fimmu.2020.00410>
- Carlin, L.M., E.G. Stamatiades, C. Auffray, R.N. Hanna, L. Glover, G. Vizcay-Barrena, C.C. Hedrick, H.T. Cook, S. Diebold, and F. Geissmann. 2013. Nr4a1-dependent Ly6C(low) monocytes monitor endothelial cells and orchestrate their disposal. *Cell.* 153:362–375. <https://doi.org/10.1016/j.cell.2013.03.010>
- Culemann, S., A. Grüneboom, and G. Krönke. 2019a. Origin and function of synovial macrophage subsets during inflammatory joint disease. *Adv. Immunol.* 143:75–98. <https://doi.org/10.1016/bs.ai.2019.08.006>
- Culemann, S., A. Grüneboom, J.Á. Nicolás-Ávila, D. Weidner, K.F. Lämmle, T. Rothe, J.A. Quintana, P. Kirchner, B. Krljanac, M. Eberhardt, et al. 2019b. Locally renewing resident synovial macrophages provide a protective barrier for the joint. *Nature.* 572:670–675. <https://doi.org/10.1038/s41586-019-1471-1>
- Davies, L.C., S.J. Jenkins, J.E. Allen, and P.R. Taylor. 2013. Tissue-resident macrophages. *Nat. Immunol.* 14:986–995. <https://doi.org/10.1038/ni.2705>
- Firestein, G.S., and I.B. McInnes. 2017. Immunopathogenesis of rheumatoid arthritis. *Immunity.* 46:183–196. <https://doi.org/10.1016/j.immuni.2017.02.006>
- Friščić, J., M. Böttcher, C. Reinwald, H. Bruns, B. Wirth, S.J. Popp, K.I. Walker, J.A. Ackermann, X. Chen, J. Turner, et al. 2021. The complement system drives local inflammatory tissue priming by metabolic reprogramming of synovial fibroblasts. *Immunity.* 54:1002–1021.e10. <https://doi.org/10.1016/j.immuni.2021.03.003>
- García-Prieto, J., R. Villena-Gutiérrez, M. Gómez, E. Bernardo, A. Pungarcía, I. García-Lunar, G. Crainiciuc, R. Fernández-Jiménez, V. Sreeramkumar, R. Bourio-Martínez, et al. 2017. Neutrophil stunning by metoprolol reduces infarct size. *Nat. Commun.* 8:14780. <https://doi.org/10.1038/ncomms14780>
- Geissmann, F., S. Gordon, D.A. Hume, A.M. Mowat, and G.J. Randolph. 2010. Unravelling mononuclear phagocyte heterogeneity. *Nat. Rev. Immunol.* 10:453–460. <https://doi.org/10.1038/nri2784>
- Ginhoux, F., and S. Jung. 2014. Monocytes and macrophages: Developmental pathways and tissue homeostasis. *Nat. Rev. Immunol.* 14:392–404. <https://doi.org/10.1038/nri3671>
- Gordon, S. 2007. The macrophage: Past, present and future. *Eur. J. Immunol.* 37:S9–S17. <https://doi.org/10.1002/eji.200737638Suppl>
- Hanna, R.N., L.M. Carlin, H.G. Hubbeling, D. Nackiewicz, A.M. Green, J.A. Punt, F. Geissmann, and C.C. Hedrick. 2011. The transcription factor NR4A1 (Nur77) controls bone marrow differentiation and the survival of Ly6C- monocytes. *Nat. Immunol.* 12:778–785. <https://doi.org/10.1038/ni.2063>
- Knab, K., D. Chambers, and G. Krönke. 2022. Synovial macrophage and fibroblast heterogeneity in joint homeostasis and inflammation. *Front. Med.* 9:862161. <https://doi.org/10.3389/fmed.2022.862161>
- Kurowska-Stolarska, M., and S. Alivernini. 2017. Synovial tissue macrophages: Friend or foe?. *RMD Open.* 3:e000527. <https://doi.org/10.1136/rmdopen-2017-000527>

- Lämmermann, T., P.V. Afonso, B.R. Angermann, J.M. Wang, W. Kastentmüller, C.A. Parent, and R.N. Germain. 2013. Neutrophil swarms require LTB₄ and integrins at sites of cell death in vivo. *Nature*. 498: 371–375. <https://doi.org/10.1038/nature12175>
- Misharin, A.V., C.M. Cuda, R. Saber, J.D. Turner, A.K. Gierut, G.K. Haines III, S. Berdnikovs, A. Filer, A.R. Clark, C.D. Buckley, et al. 2014. Non-classical Ly6C(-) monocytes drive the development of inflammatory arthritis in mice. *Cell Rep*. 9:591–604. <https://doi.org/10.1016/j.celrep.2014.09.032>
- Moreno, S.G. 2018. Depleting macrophages in vivo with clodronate-liposomes. *Methods Mol. Biol.* 1784:259–262. https://doi.org/10.1007/978-1-4939-7837-3_23
- Richards, P.J., A.S. Williams, R.M. Goodfellow, and B.D. Williams. 1999. Liposomal clodronate eliminates synovial macrophages, reduces inflammation and ameliorates joint destruction in antigen-induced arthritis. *Rheumatology*. 38:818–825. <https://doi.org/10.1093/rheumatology/38.9.818>
- Solomon, S., N. Rajasekaran, E. Jeisy-Walder, S.B. Snapper, and H. Illges. 2005. A crucial role for macrophages in the pathology of K/B x N serum-induced arthritis. *Eur. J. Immunol.* 35:3064–3073. <https://doi.org/10.1002/eji.200526167>
- Summan, M., G.L. Warren, R.R. Mercer, R. Chapman, T. Hulderman, N. Van Rooijen, and P.P. Simeonova. 2006. Macrophages and skeletal muscle regeneration: A clodronate-containing liposome depletion study. *Am. J. Physiol. Regul. Integr. Comp. Physiol.* 290:R1488–R1495. <https://doi.org/10.1152/ajpregu.00465.2005>
- Udalova, I.A., A. Mantovani, and M. Feldmann. 2016. Macrophage heterogeneity in the context of rheumatoid arthritis. *Nat. Rev. Rheumatol.* 12: 472–485. <https://doi.org/10.1038/nrrheum.2016.91>
- Uderhardt, S., A.J. Martins, J.S. Tsang, T. Lämmermann, and R.N. Germain. 2019. Resident macrophages cloak tissue microlesions to prevent neutrophil-driven inflammatory damage. *Cell*. 177:541–555.e17. <https://doi.org/10.1016/j.cell.2019.02.028>
- van Rooijen, N., A. Sanders, and T.K. van den Berg. 1996. Apoptosis of macrophages induced by liposome-mediated intracellular delivery of clodronate and propamidine. *J. Immunol. Methods*. 193:93–99. [https://doi.org/10.1016/0022-1759\(96\)00056-7](https://doi.org/10.1016/0022-1759(96)00056-7)
- Wipke, B.T., and P.M. Allen. 2001. Essential role of neutrophils in the initiation and progression of a murine model of rheumatoid arthritis. *J. Immunol.* 167:1601–1608. <https://doi.org/10.4049/jimmunol.167.3.1601>
- Yona, S., K.W. Kim, Y. Wolf, A. Mildner, D. Varol, M. Breker, D. Strauss-Ayali, S. Viukov, M. Guilliama, A. Misharin, et al. 2013. Fate mapping reveals origins and dynamics of monocytes and tissue macrophages under homeostasis. *Immunity*. 38:79–91. <https://doi.org/10.1016/j.immuni.2012.12.001>

Supplemental material

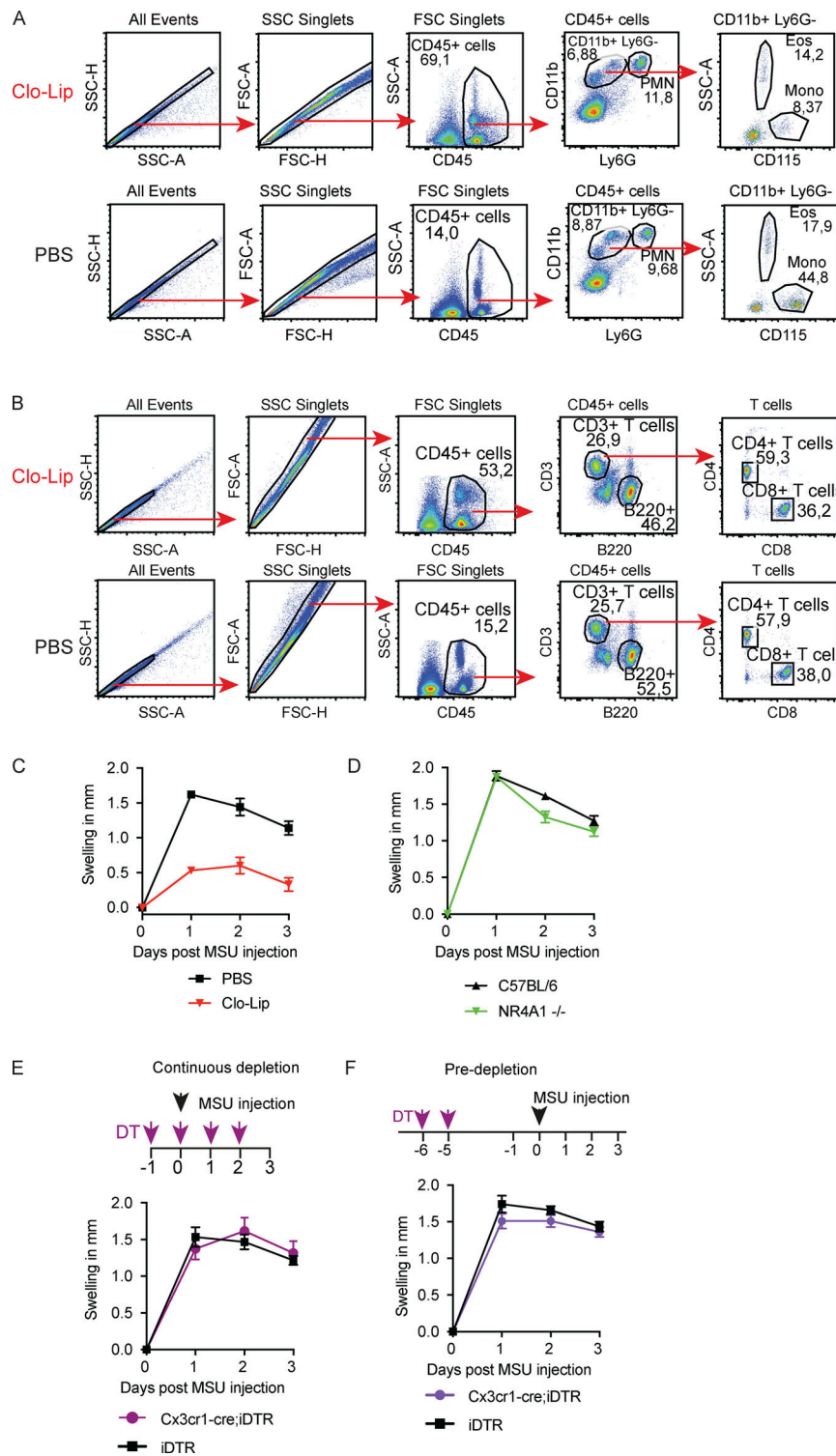


Figure S1. **Clo-Lip treatment depletes MoPh and results in MoPh-independent anti-inflammatory effects in MSU-induced gouty arthritis. (A and B)** Gating strategy for CD45⁺CD11b⁺Ly6G⁺ PMN, CD45⁺CD11b⁺CD115⁺ monocytes, CD45⁺CD11b⁺SSC^{high} eosinophils, CD45⁺B220⁺ B cells, CD3⁺CD4⁺ T cells, and CD3⁺CD8⁺ T cells in mouse blood 24 h after i.v. injection of 200 μ l Clo-Lip or PBS. **(C)** Clinical development of MSU-induced gouty arthritis in mice treated with 200 μ l Clo-Lip or PBS as control. Clo-Lip were administered 24 h before injection of 50 μ l MSU (20 mg/ml). Inflammation was evaluated by measurement of paw swelling ($n = 5$ per group). **(D)** Clinical development of MSU-induced gouty arthritis in NR4A1^{-/-} mice or C57BL/6 wild-type mice. Inflammation was evaluated by measurement of paw swelling ($n = 4$ per group). **(E and F)** Clinical development of MSU-induced gouty arthritis in DT-treated Cx3cr1-cre;iDTR mice or DT-treated iDTR control mice. **(E)** For continuous depletion, mice received DT every day starting 1 d before MSU injection ($n = 6$ per group). **(F)** For pre-depletion, DT was injected only twice 6 d before MSU injection. Inflammation was evaluated by measurement of paw swelling (Cx3cr1-cre;iDTR $n = 5$, iDTR $n = 6$). Experiments in C–F were performed one time. Data are mean \pm SEM. Numbers indicated in flow cytometry plots represent the percentage of the parent population.

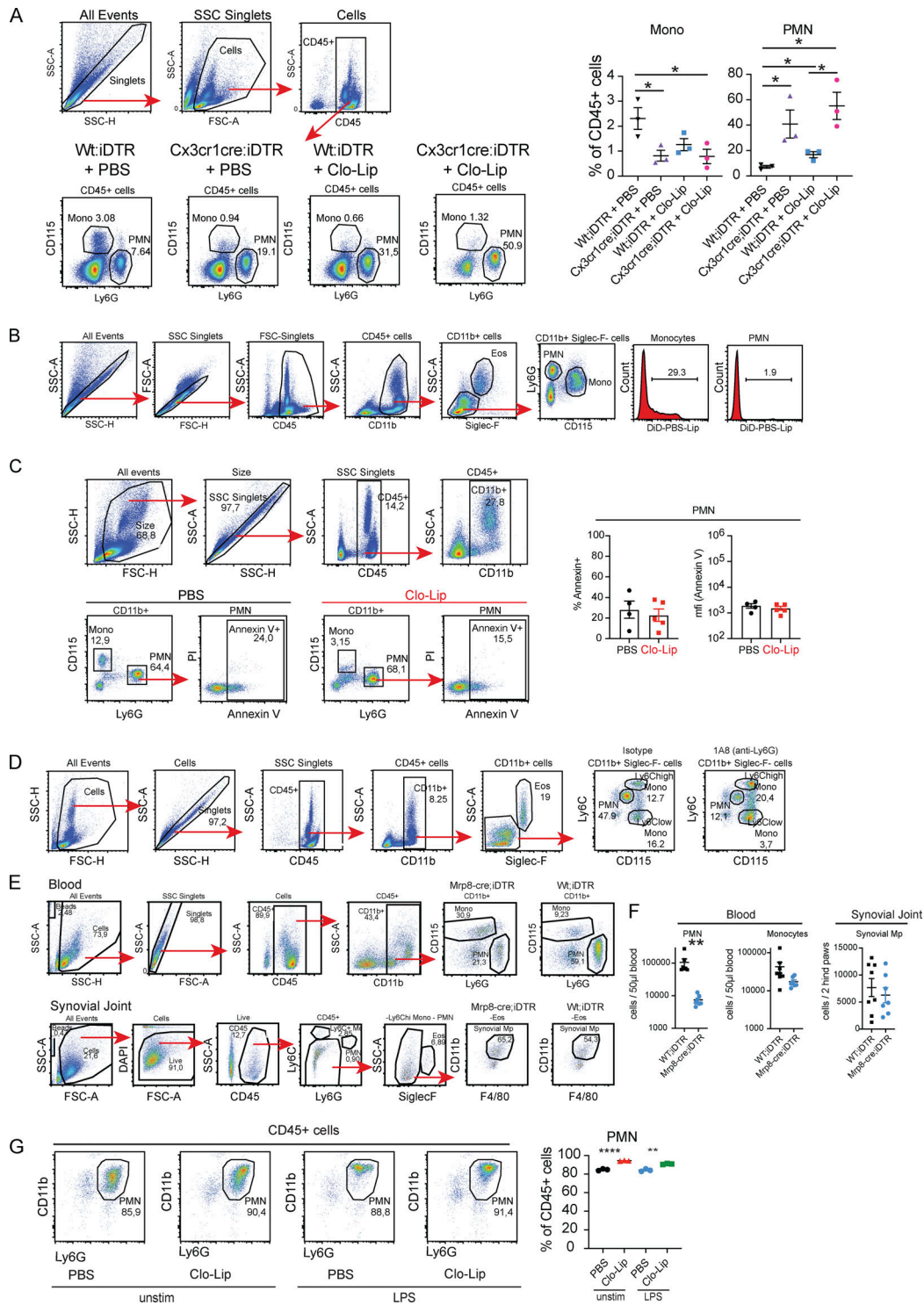


Figure S2. Characterization of leukocyte subsets upon Clo-Lip treatment and PMN depletion, respectively. (A) Flow cytometry analysis of blood of DT-treated Cx3cr1-cre;iDTR or DT-treated iDTR mice, which received either Clo-Lip or PBS 24 h before analysis. Monocytes were defined as CD45⁺ and CD115⁺, and PMN were defined as CD45⁺ and Ly6G⁺ ($n = 3$ per group). Data are mean \pm SEM; two-tailed Student's t test; *, $P < 0.05$. (B) Flow cytometry of blood of C57BL/6 mice 24 h after injection of DiD-labeled PBS-loaded liposomes (DiD-PBS-Lip) showing the uptake of PBS-liposomes by CD45⁺CD11b⁺Ly6G⁺ PMN and CD45⁺CD11b⁺CD115⁺ monocytes. (C) Flow cytometry assessing apoptosis of blood PMN via Annexin V and propidium iodide (PI) staining 24 h after i.v. Clo-Lip injection (PBS-treated mice: $n = 4$; Clo-Lip-treated mice: $n = 5$). Data are mean \pm SEM. (D) Gating strategy of blood of C57BL/6 mice 24 h after treatment with PMN-depleting 1A8 antibody (anti-Ly6G) or isotype control. (E and F) Gating strategy (E) and quantification of monocytes and PMN in blood (F) as well as synovial macrophages of hind paws of MRP8-cre;iDTR and iDTR wild-type control mice 24 h after DT administration ($n = 7-8$ per group). Data are mean \pm SEM; Student's t test; **, $P = 0.0063$. (G) Flow cytometry of enriched PMN harvested from five PBS- or five Clo-Lip-treated (i.v., 24 h) mice 6 h after ex vivo incubation with or without LPS. Data from three technical replicates of each condition are shown. Student's t test; **, $P < 0.0015$; ****, $P < 0.0001$. Experiments in A and D were performed at least two times. Experiments in B and E-G were performed once.